Ionics (2022) 28:669–682
https://doi.org/10.1007/s11581-021-04374-6

ORIGINAL PAPER

Cyclodextrin polymers as effective water-soluble binder with enhanced cycling performance for $Li_2ZnTi_3O_8$ anode in lithium-ion batteries

Long Wang[1] · Zheng Han[1] · Qiang Weng[2] · Tao Liu[3] · Zhiyuan Tang[3] · Haoqing Tang[1]

Received: 24 September 2021 / Revised: 3 November 2021 / Accepted: 17 November 2021 / Published online: 30 November 2021

Abstract

Polymeric binders play an important role in maintaining the integrity of electrodes and improving the electrochemical performance of batteries. Unlike binders soluble in organic solvents, water-soluble binders are environmentally friendly and easy to recycle. In this work, a comparative study on the effects of water-soluble cyclodextrin and organic-based PVDF binders on the Li^+ intercalation/deintercalation of lithium-ion batteries with $Li_2ZnTi_3O_8$ anode is conducted for the first time. Compared to α-cyclodextrin, γ-cyclodextrin, and PVDF, LZTO with β-cyclodextrin binder exhibits larger Li^+ storage capacity, better cycle stability, rate capability, and higher Coulombic efficiency, possessing a high electrical conductivity, low charge transfer resistance, and fast lithium-ion diffusion coefficient. β-Cyclodextrin water-soluble binder not only makes the active material difficult to separate from the current collector and facilitates favorable electrochemical kinetics but also maintains good cycle stability at high temperatures. Utilizing these advantageous features, β-Cyclodextrin-based LZTO electrode shows markedly improved reversible Li^+ storage performance compared to those of other binder cases.

Keywords Lithium-ion battery · Lithium zinc titanate · Binder · Cyclodextrin · Electrochemical performance

Introduction

High-performance energy storage devices play a significant role in portable electronic devices, wearable devices, and precision instruments. Up to now, a variety of innovative electrochemical energy storage devices have been continuously developed. Among these different devices, rechargeable lithium-ion batteries (LIBs) have the exceptional electrochemical performance to make them receive particular attention [1–3]. Currently, the electrode of conventional LIBs is composed of active material, polymer binder, and conductive carbon. In recent decades, active materials with different crystal structures have been used in LIBs, such as $LiCoO_2$, $Li_3V_2(PO_4)_3$, $LiFePO_4$, $LiNi_{0.5}Mn_{1.5}O_4$, $Li_4Ti_5O_{12}$, and graphite [4–9]. Although active materials directly determine the energy and power density of the LIBs, the inactive polymer binders also play a critical role in facilitating electron transport and ion diffusion, holding the integrity of the physical structure of electrode and maintaining the stable long cycling performance for cells [10–13]. Therefore, a battery with superior electrochemical performance must rely on high-performance binder.

As for commercial LIBs, polyvinylidene fluoride (PVDF) is usually selected as the binder for the active material in electrodes, which has the good binding capability, thermal stability, and the ability to adsorb organic electrolyte [14, 15]. However, PVDF has obvious shortcomings in physical properties and chemical reactions: (1) need non-environmentally friendly solvent. PVDF is required to dissolved in N-Methyl Pyrrolidone (NMP), and NMP is volatile and toxic; (2) prone to chemical reactions and produce by-products. PVDF can react with lithium metal and Li_xC_6 to form LiF and -(-C = C-F)- on the electrode surface via an

Long Wang and Zheng Han contributed equally to this work

✉ Haoqing Tang
tanghaoqing@126.com

[1] School of Materials Science and Engineering, Hebei University of Engineering, Handan, Hebei 056038, People's Republic of China

[2] School of Materials Science and Engineering, Shaanxi Normal University, Xi'an, Shaanxi 710119, People's Republic of China

[3] School of Chemical Engineering and Technology, Tianjin University, Tianjin 300072, People's Republic of China

exothermic reaction, which causes thermal runaway [16]; (3) PVDF is easy to swell and has low flexibility, which causes active particles to fall off from the current collector during long cycles [17]; (4) PVDF is costly and cannot be recycled effectively [18]. To avoid these obvious shortcomings, water-soluble binders become a good substitute among different binder systems.

Compared with traditional PVDF binder, water-based binders have unique advantages [19], including the following points: (1) the mixing and stirring time with active materials and conductive carbon is reduced by 50%; (2) it is not easy to decompose at low temperatures (< 300 °C); (3) it has good freeze–thaw resistance and excellent grinding stability; and (4) it can be easily disposed at the end of battery life and environmentally friendly. So far, a variety of water-based binders have been discovered and used in lithium-ion batteries and Li–S batteries [20]. CMC is a water-soluble material, and CMC-based binders have been used in various electrode active materials, such as graphite, SnO_2, $Li_4Ti_5O_{12}$, and $LiFePO_4$ [21–23], and the electrochemical performance has been significantly improved. Li et al. chose sodium carboxymethyl cellulose (CMC-Na) as the water-soluble binder for lithium-ion batteries with good electrochemical performance [24]. Furthermore, aqueous polymer binders such as CMC/SBR, PAA, SA, and LA-132 [25–28] were also used as binders for sulfur in Li–S batteries. These binders can use polymer functional groups to form covalent bonds with sulfur particles to obtain stable electrodes and improve charge and discharge performance. Besides, carboxymethyl cellulose lithium [29], gelatin [30], carboxymethyl fenugreek gum [31], poly(acrylic acid) [32], poly(methacrylic acid) [33], poly(vinyl acid) [34], chitosan and chitosan oligosaccharide [35], alginate [36], polymide [37], G4CMP [38], and sodium alginate [39] have been selected as binders, which are apparently improve rate properties and long cycling performance.

In order to solve the structural instability of Si anode in lithium-ion batteries during multiple cycles, binders with different structures and functions have been designed. Hu et al. constructed a binder system with a double network structure to maintain the Si electrode structure and improve electrochemical performance by dispersing and releasing unfavorable stress [40]. Jiao et al. designed a double-wrapped binder with polyacrylic acid (PAA) inside and bifunctional polyurethane (BFPU) outside to address the large inner stress of silicon anode with drastic volume changes during cycling, achieving a long cycling life [41]. Hu and coworkers reported a gradient hydrogen-bonding binder, which effectively release the large stress of silicon via the sequential bonding cleavage [42].

Cyclodextrin (abbreviated as CD) is a general term for cyclic oligosaccharides produced by amylose under the action of enzymes and contains 6–12 D-glucopyranose units. Among them, molecules with 6, 7, and 8 glucose units are of great practical significance, which is called α-cyclodextrin, β-cyclodextrin, and γ-cyclodextrin, respectively. Herein, we introduced for the first time cyclodextrin polymer as a new $Li_2ZnTi_3O_8$ anode water-based binder. Compared with traditional binders, there are abundant alcoholic hydroxyl groups on the outer surface of the cavity. These alcoholic hydroxyl groups can make it not only easily soluble in water, but also can be effectively combined with active particles through noncovalent interactions, thereby improving electrochemical performance [11]. Also, cyclodextrin has good wettability to the electrolyte and can reduce the interface resistance, thereby improving the high rates of charge–discharge performance of lithium-ion batteries.

Here is a brief introduction to $Li_2ZnTi_3O_8$ anode material: cubic spinel belongs to titanium-based materials, and the available capacity is higher than commercialized $Li_4Ti_5O_{12}$. The three-dimensional network formed by Li–O and Ti–O is propitious to the Li^+ reversible intercalation/deintercalation. Moreover, the operating potential of $Li_2ZnTi_3O_8$ is around 0.6 V, which can avoid dendritic lithium growing. Based on the above advantages, it is regarded as promising anode candidate material in LIBs.

Herein, we studied systemically that the effects of the binders α-cyclodextrin, β-cyclodextrin, and γ-cyclodextrin on electrochemical performance include long cycling stability, rate capability, and megathermal performance of $Li_2ZnTi_3O_8$ (the specific molecular structures of binders are presented in Fig. 1). Furthermore, the impacts of the binders in the high temperature cycle performance were discussed. For comparison, the cycling performance under different test conditions of $Li_2ZnTi_3O_8$ with PVDF binder and NMP solvent has also been investigated.

Experimental

Synthesis of $Li_2ZnTi_3O_8$ active materials

Here, all the raw materials in preparation procedure were used directly without further purification. $Li_2ZnTi_3O_8$ electrode active material was synthesized through the solid-state calcination process at high temperature. A typical procedure is as following. 1.3658 g of TiO_2, 1.2512 g of $Zn(CH_3COO)_2{\cdot}2H_2O$, 0.4212 g of Li_2CO_3, and 25 mL of anhydrous ethanol were mixed and ball-milled in planetary ball mill at 25 °C for 4 h. The white mixture was obtained via evaporation at 80 °C for 12 h in electric drying oven. Finally, $Li_2ZnTi_3O_8$ active material was prepared by grinding white dry powder and followed by sintering at 800 °C for 5 h in muffle furnace under air atmosphere.

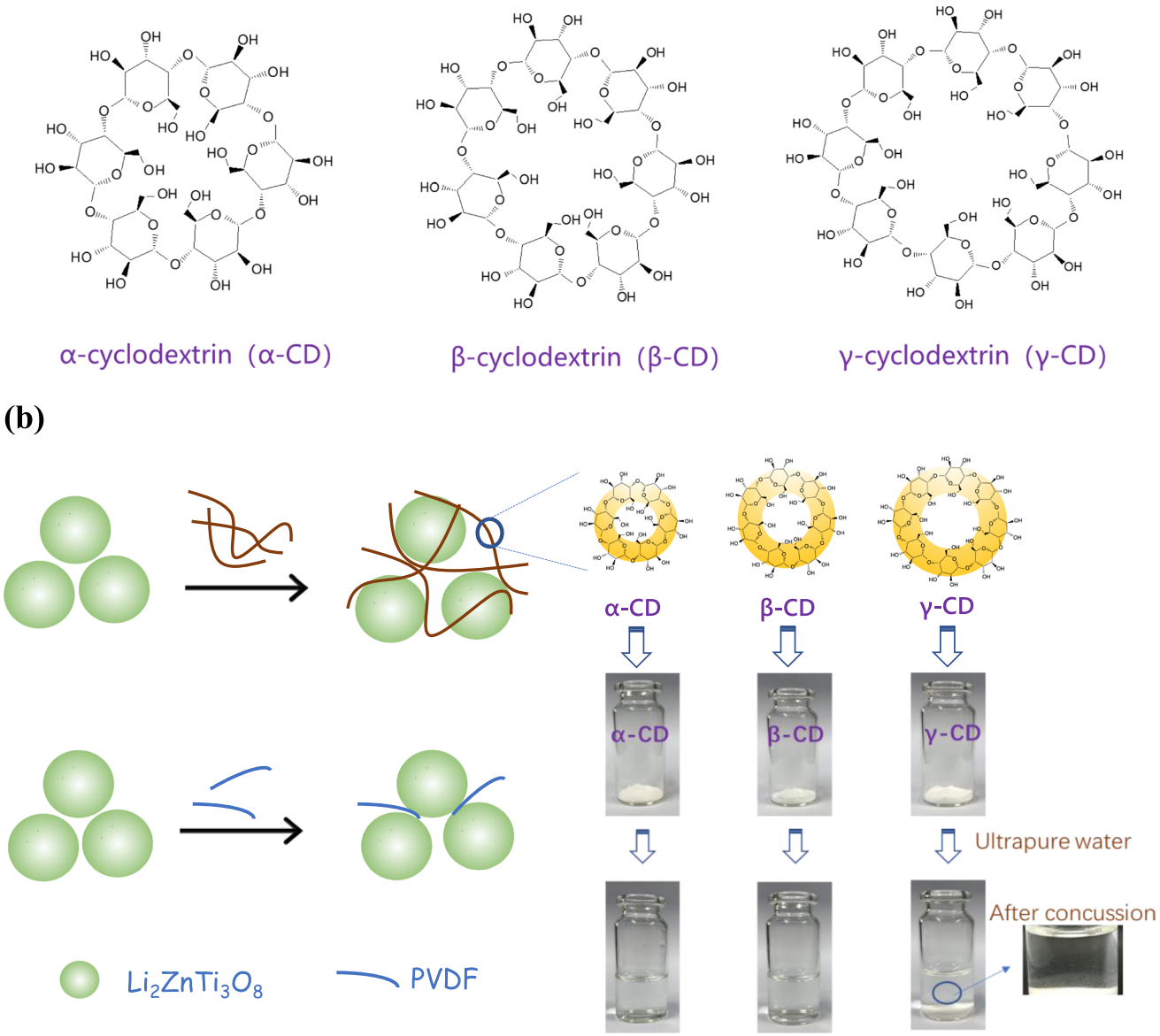

Fig. 1 **a** Structural formulas and graphical representations of α-cyclodextrin, β-cyclodextrin, and γ-cyclodextrin binders used in this study. **b** Schematic illustration of $Li_2ZnTi_3O_8$ and binder configurations for $Li_2ZnTi_3O_8$-cyclodextrin and $Li_2ZnTi_3O_8$-PVDF. The phenomenon of cyclodextrin dissolved in ultrapure water after concussion

Materials characterizations

X-ray diffraction (Rigaku D/max 2550, Cu Ka radiation) and Fourier transform infrared spectrometer (Vertex70, BRUKER OPTICS, 4000–400 cm^{-1} region) were conducted on the as-prepared $Li_2ZnTi_3O_8$ and binders to confirm their structure. Brunauer–Emmett–Teller surface areas and pore size distribution (Barrett-Joyner-Halenda model) were tested by BELSORP-mini (Microtrac BEL, analysis adsorptive: N_2). Field mission scanning electron microscopy (Philips Quanta 200) and high-resolution transmission electron microscopy (JEOL JEM-2100F) were used for micromorphology determination. X-ray photoelectron spectroscopy (XPS, ESCALAB Xi^+, Thermo Fisher Scientific) was used for molecular structure and atomic valence of samples.

Electrochemical measurements

The electrochemical properties of $Li_2ZnTi_3O_8$ with different binders were evaluated using CR2032 coin cells assembled in a high purity argon filled glove box, with H_2O and O_2 concentration being controlled to be lower

1 ppm. The $Li_2ZnTi_3O_8$ electrodes is composed of 80 wt% active materials, 10 wt% acetylene black, and 10 wt% binder (α-cyclodextrin, β-cyclodextrin, and γ-cyclodextrin) and evenly mixed in an agate mortar. After that, a certain amount of ultrapure water was added into the mixed powders and continued to stir for 20 min. The resultant slurries were coated on Cu foil and dried at 120 °C for 12 h under vacuum. The CR2032 coin half cells consist of four parts, which are $Li_2ZnTi_3O_8$ cathode, Li foil anode, microporous polypropylene (Celgard 2300) membrane, and organic electrolyte containing 1.0 M $LiPF_6$ in EC/DMC = 50/50 (v/v). As a comparison, the water-soluble cyclodextrin binders replaced by polyvinylidene difluoride (PVDF) dissolved in N-methyl pyrrolidone (NMP). Moreover, the loading of the active materials is 1.0 ~ 1.2 mg for each tested coin cells.

Electrochemistry cycling tests were performed between 0.05 and 3.0 V using Neware Battery Charge and Discharge Test System at different current densities. Electrochemical impedance spectroscopy (EIS) tests were carried out on a CHI660C electrochemical workstation.

Results and discussion

The structural formulas of α-cyclodextrin, β-cyclodextrin, and γ-cyclodextrin are displayed in Fig. 1a. α-Cyclodextrin, β-cyclodextrin, and γ-cyclodextrin binders are composed of molecules of 6, 7, and 8 glucose molecules, respectively, and has a cone-shaped hollow cylindrical three-dimensional ring structure. In the hollow structure, the outer side is composed of secondary hydroxyl groups and primary hydroxyl groups, which is hydrophilic, while the cavity is formed with hydrophobic regions due to the shielding effect of C-H bonds. The formation processes of both LZTO with PVDF binder and LZTO with cyclodextrin are shown in Fig. 1b. First of all, solid cyclodextrin was added to ultrapure water to form a transparent and uniform solution. Because the γ-cyclodextrin molecule has a large cavity pore, it is easy to contact with other molecules to affect solubility. Besides, it can be seen from the γ-cyclodextrin that some γ-cyclodextrin solids still exist after vigorous stirring. In the second step, LZTO is mixed with PVDF, α-cyclodextrin, β-cyclodextrin, and γ-cyclodextrin binders. The one-dimensional linear structure of cyclodextrin can be in better contact with the active material particles, while the cavity structure leaves interval between the particles, allowing electrolyte to fully penetrate into particles surface. In contrast, PVDF is in a linear structure contact with LZTO active materials and has poor adhesion.

As shown in Fig. 2a, the crystal structure of pristine $Li_2ZnTi_3O_8$ is illustrated. All the main diffraction peaks can be indexed to the cubic spinel $Li_2ZnTi_3O_8$ structure (JCPDS no. 44–1037) with a space group [$P4_332$], and no extra diffraction peaks (e.g. TiO_2, ZnO, and Li_2O) are detected according to the XRD results [43]. N_2 adsorption/desorption characterization based on Brunauer–Emmett–Teller and Barrett-Joyner-Halenda were used for analyzing specific surface area and pore size distribution of pristine $Li_2ZnTi_3O_8$ nanoparticles. The specific surface area of $Li_2ZnTi_3O_8$ is 3.0314 $m^2\ g^{-1}$ (Fig. 2b), and the average diameter of pores is 8.94 nm (Fig. 2c). Based on the result of SEM (Fig. 2d), $Li_2ZnTi_3O_8$ has a relatively obvious agglomeration phenomenon after high temperature calcination, resulting in a lower specific surface area. Furthermore, the stacked pores between $Li_2ZnTi_3O_8$ particles are clearly visible, which is beneficial to the penetration of electrolyte and the transmission of lithium ions. As shown in TEM image (Fig. 2e), the $Li_2ZnTi_3O_8$ powder consists of irregular particles with diameters of 80–150 nm. In the high-resolution HRTEM image (Fig. 2f), the lattice spacing of 0.481 nm can be observed clearly, corresponding to the (111) plane of the cubic spinel structure of $Li_2ZnTi_3O_8$ as indicated in XRD pattern.

The SEM images in Fig. 3a–d reveal the microscopic morphology of various binders. The microscopic morphology of α-cyclodextrin (a), β-cyclodextrin (b), and γ-cyclodextrin (c) is quite different from PVDF, showing irregular blocky solids and large diameter. In contrast, the microscopic morphology of PVDF is formed by the aggregation of smaller particles. Figure 3e–h shows the morphology of LZTO electrode pole piece with α-cyclodextrin (e), β-cyclodextrin (f), γ-cyclodextrin (g), and PVDF (h) binders. It can be clearly seen that the cyclodextrin binders are uniformly mixed with LZTO particles, and there are more pores between the particles, which facilitates the rapid migration of lithium ions and the penetration of electrolyte. Different from the cyclodextrin binder, the surface of the LZTO pole piece based on PVDF binder forms a relatively compact structure, which is detrimental to the function of lithium ion and electrolyte.

The potential versus capacity profiles in the first cycle for LZTO with β-cyclodextrin binder and PVDF binder are presented in Fig. 4a–c and g–i. Obviously, the contour of charge and discharge curves of LZTO with β-cyclodextrin binder and PVDF binder is basically the same, indicating that the binder has no influence on the electrochemical reaction process. For both electrodes, the discharge and charge capacities gradually decreased with increase in the galvanostatic discharge–charge current densities. The LZTO with β-cyclodextrin binder exhibited obviously better discharge/charge capacities than that of the PVDF binder at 0.1 A g^{-1}, 1.0 A g^{-1}, and 3.0 A g^{-1}, respectively, which can be attributed to the unique physical characteristics. Moreover, the voltage plateau differences between charge voltage and discharge voltage of β-cyclodextrin-based LZTO electrode are 0.81 V, 1.03 V, and 1.27 V at 0.1 A g^{-1}, 1.0 A g^{-1}, and 3.0 A g^{-1}, respectively, while

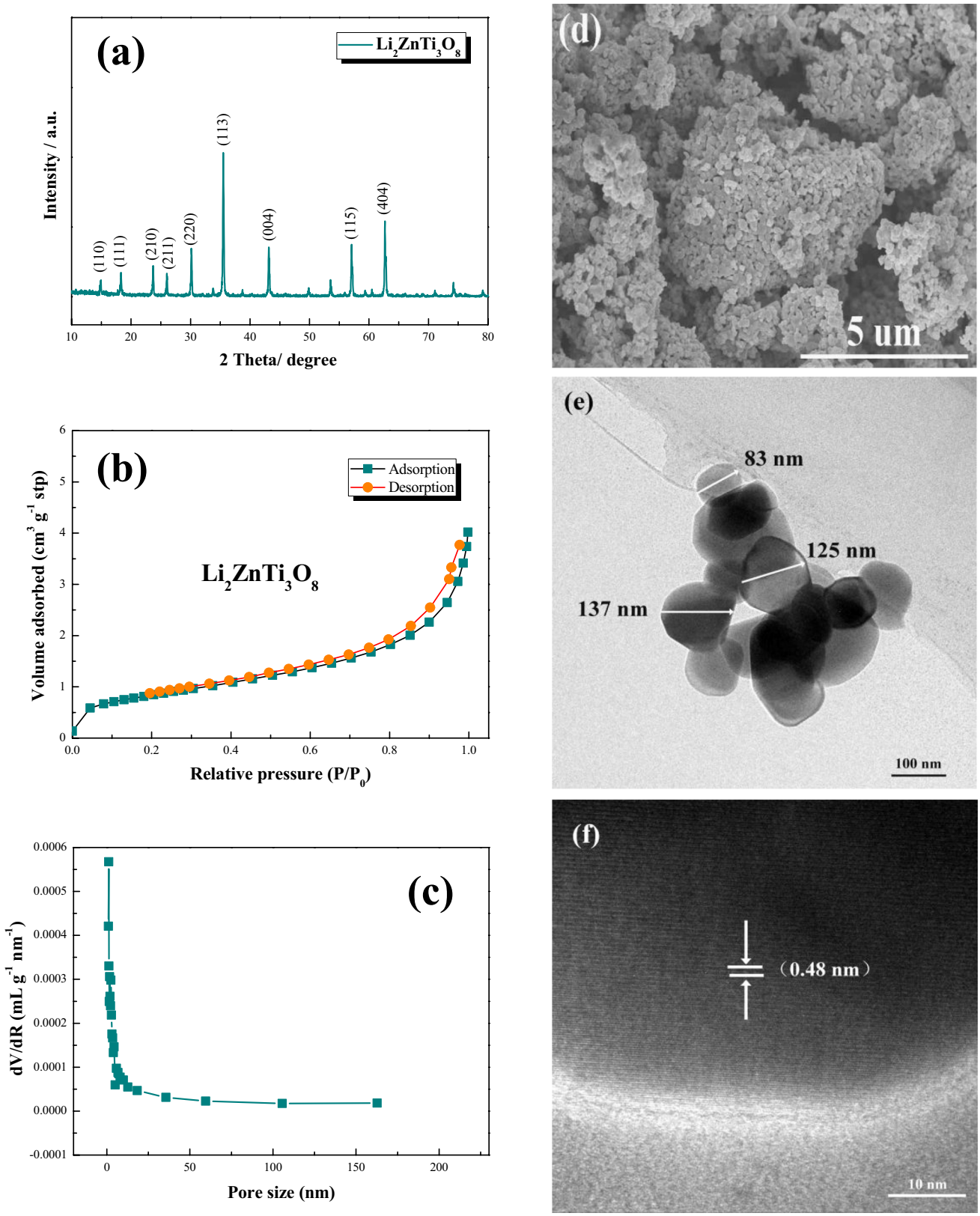

Fig. 2 Characterizations of pristine $Li_2ZnTi_3O_8$ nanoparticles. **a** Typical XRD pattern. **b** N_2 adsorption/desorption isotherm. **c** Pore size distribution. **d** SEM image. **e** TEM image. **f** HRTEM image

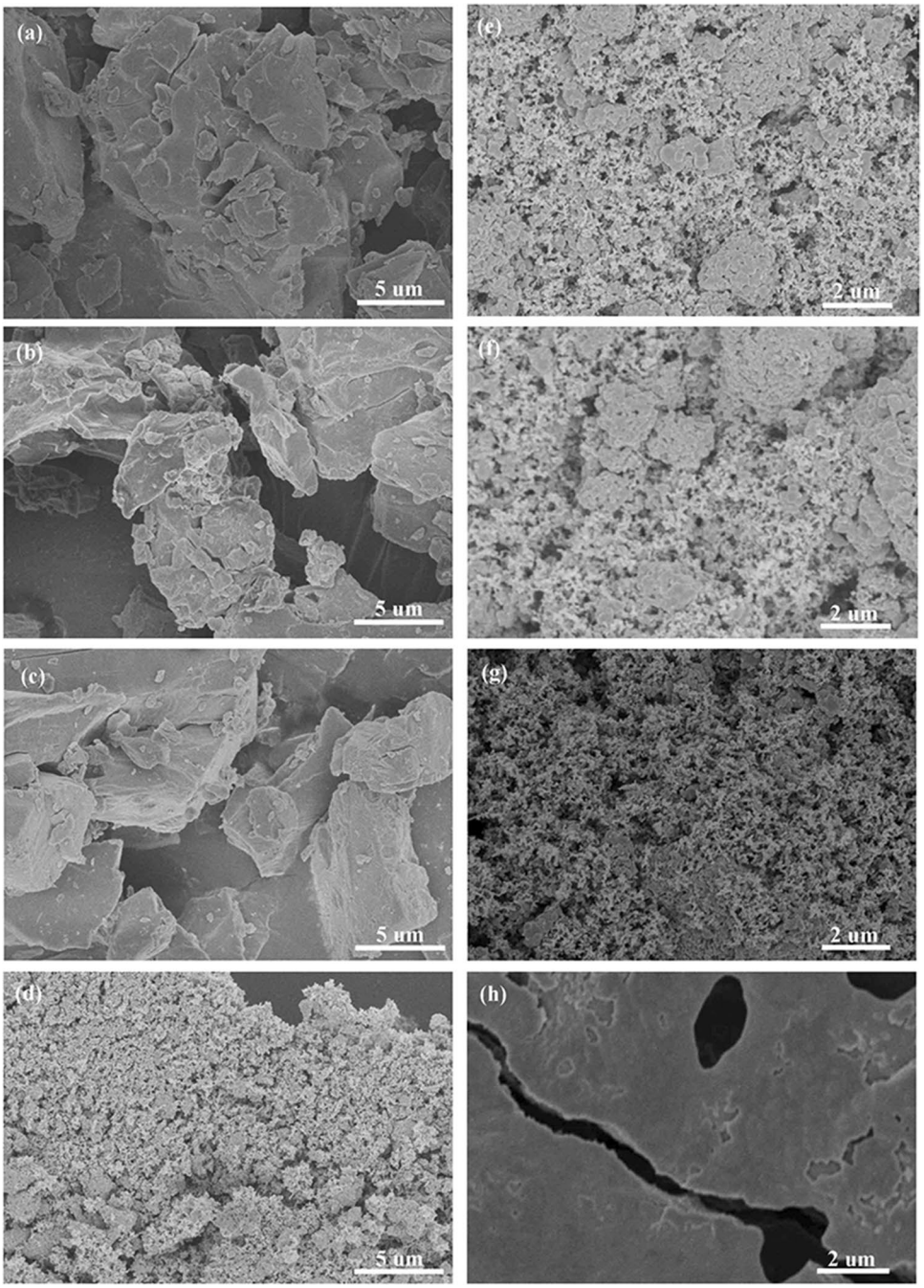

Fig. 3 SEM images (top view) of α-cyclodextrin, β-cyclodextrin, γ-cyclodextrin, and PVDF binders, respectively (**a**–**d**); SEM images (top view) of LZTO electrode pole piece surface using different binders: **e** α-cyclodextrin, **f** β-cyclodextrin, **g** γ-cyclodextrin, and **h** PVDF binders

of PVDF-based LZTO electrode are 0.81 V, 1.07 V, and 1.48 V at 0.1 A g^{-1}, 1.0 A g^{-1}, and 3.0 A g^{-1}, respectively. It is obvious that β-cyclodextrin-based LZTO electrode has smaller polarization compared with PVDF-based LZTO electrode, demonstrating better kinetic process and desirable electrochemical reversibility [44]. Figure 4d–f and j–l display the corresponding differential capacities vs. voltage plots of LZTO with β-cyclodextrin and PVDF binders. It can be seen intuitively from the curve outline in the figure that one couple of dQ/dV peak higher 1.0 V (vs. Li/Li^+), corresponding to Li^+ intercalation and delithiation. Besides, one more peak below 0.8 V (vs. Li/Li^+) can be attributed to multiple restoration of Ti^{4+} [45, 46]. Furthermore, based on the redox peak voltage difference, the LZTO with β-cyclodextrin binder electrode has a smaller voltage difference, and the result is consistent with the charge and discharge curves, which improve the charge-transfer kinetics. Fig. S1 shows the charge–discharge profiles and corresponding dQ/dV profiles of LZTO with α-cyclodextrin (a) and γ-cyclodextrin (b). Through detailed comparison, the polarization of LZTO with α-cyclodextrin and γ-cyclodextrin is smaller

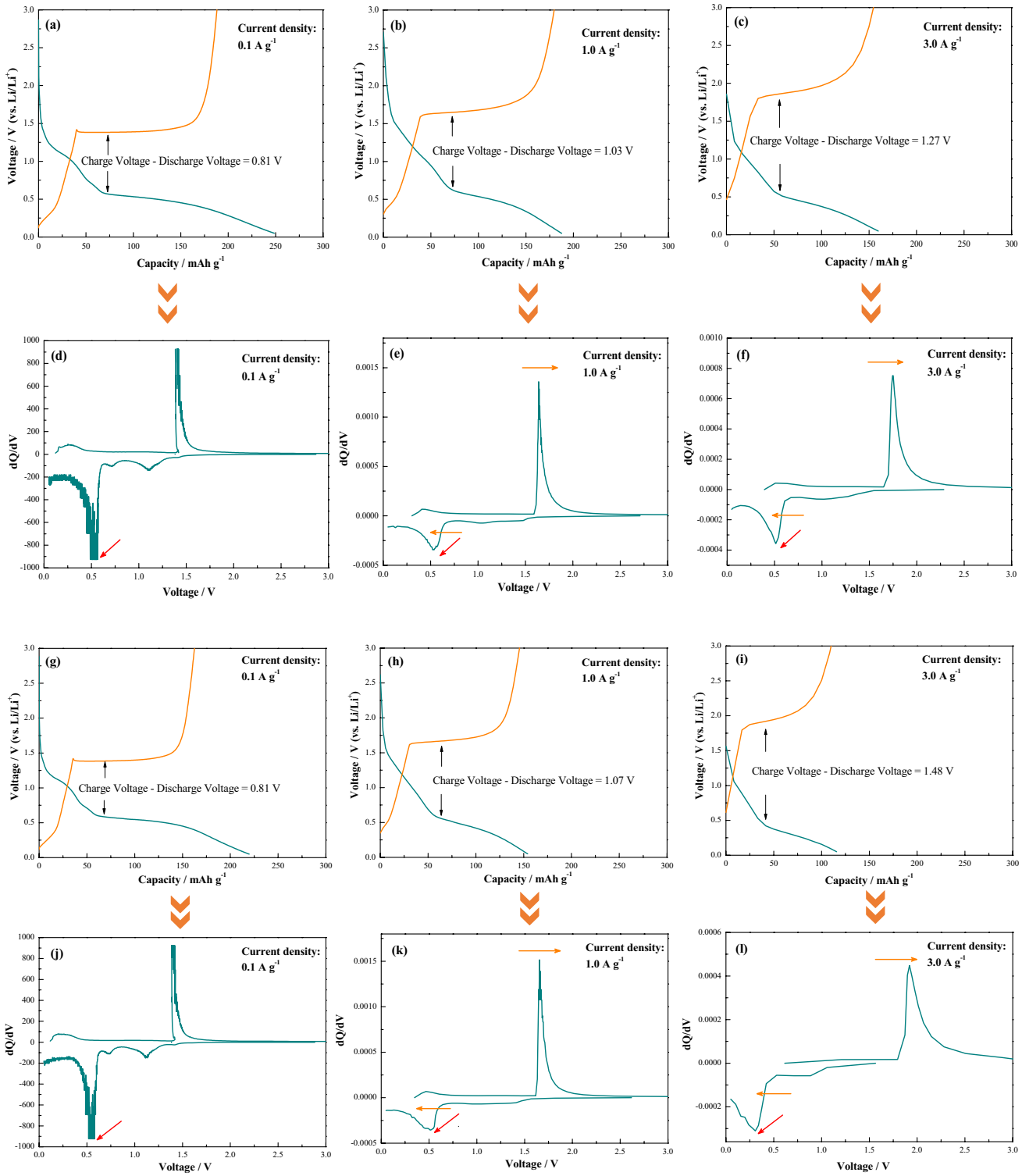

Fig. 4 Charge–discharge profiles of LZTO with β-cyclodextrin binder (**a–c**) and PVDF binder (**g–i**) at the first cycle under various current densities (0.1 A g^{-1}, 1.0 A g^{-1}, and 3.0 A g^{-1}). Discharge–charge curves and corresponding dQ/dV profiles of LZTO with β-cyclodextrin binder (**d–f**) and PVDF binder (**j–l**)

than and close to LZTO with PVDF, further indicating that the binder structure has a direct impact on electrochemical performance.

The cycling performances of LZTO electrode with four different binders (α-cyclodextrin, β-cyclodextrin, γ-cyclodextrin, and PVDF) were investigated by a series of galvanostatic discharge–charge process at room temperature. As displayed in Fig. 5a, the LZTO electrode with β-cyclodextrin binder shows an initial discharge capacity of 270.9 mAh g^{-1}, which is higher than that using α-cyclodextrin (220.9 mAh g^{-1}), γ-cyclodextrin (225.5 mAh g^{-1}), and PVDF (203.3 mAh g^{-1}) binders at current density of 0.1 A g^{-1}. Upon cycling, the LZTO electrode with β-cyclodextrin binder still exhibits a higher discharge capacity of 212.9 mAh g^{-1} than that of the α-cyclodextrin (190.1 mAh g^{-1}), γ-cyclodextrin (188.9 mAh g^{-1}), and PVDF (175.3 mAh g^{-1}) binders after 100 galvanostatic discharge–charge cycles at current density of 0.1 A g^{-1}. Even at high current densities, excellent discharge capacity and long cycling stability are also achieved for LZTO electrode with β-cyclodextrin binder (Fig. 5b–e). The 500th discharge capacities of the LZTO electrode with β-cyclodextrin binder are about 169.1 mAh g^{-1}, 166.5 mAh g^{-1}, 140.2 mAh g^{-1}, and 90.9 mAh g^{-1} at current densities of 1.0 A g^{-1}, 2.0 A g^{-1}, 4.0 A g^{-1}, and 5.0 A g^{-1}, respectively, much better than the LZTO electrode with α-cyclodextrin (133.3 mAh g^{-1}, 124.9 mAh g^{-1}, 97.8 mAh g^{-1}, and 81.6 mAh g^{-1}), γ-cyclodextrin (139.6 mAh g^{-1}, 118.1 mAh g^{-1}, 110.8 mAh g^{-1}, and 78.2 mAh g^{-1}), and PVDF (108.1 mAh g^{-1}, 72.9 mAh g^{-1}, 49.4 mAh g^{-1}, and 38.5 mAh g^{-1})

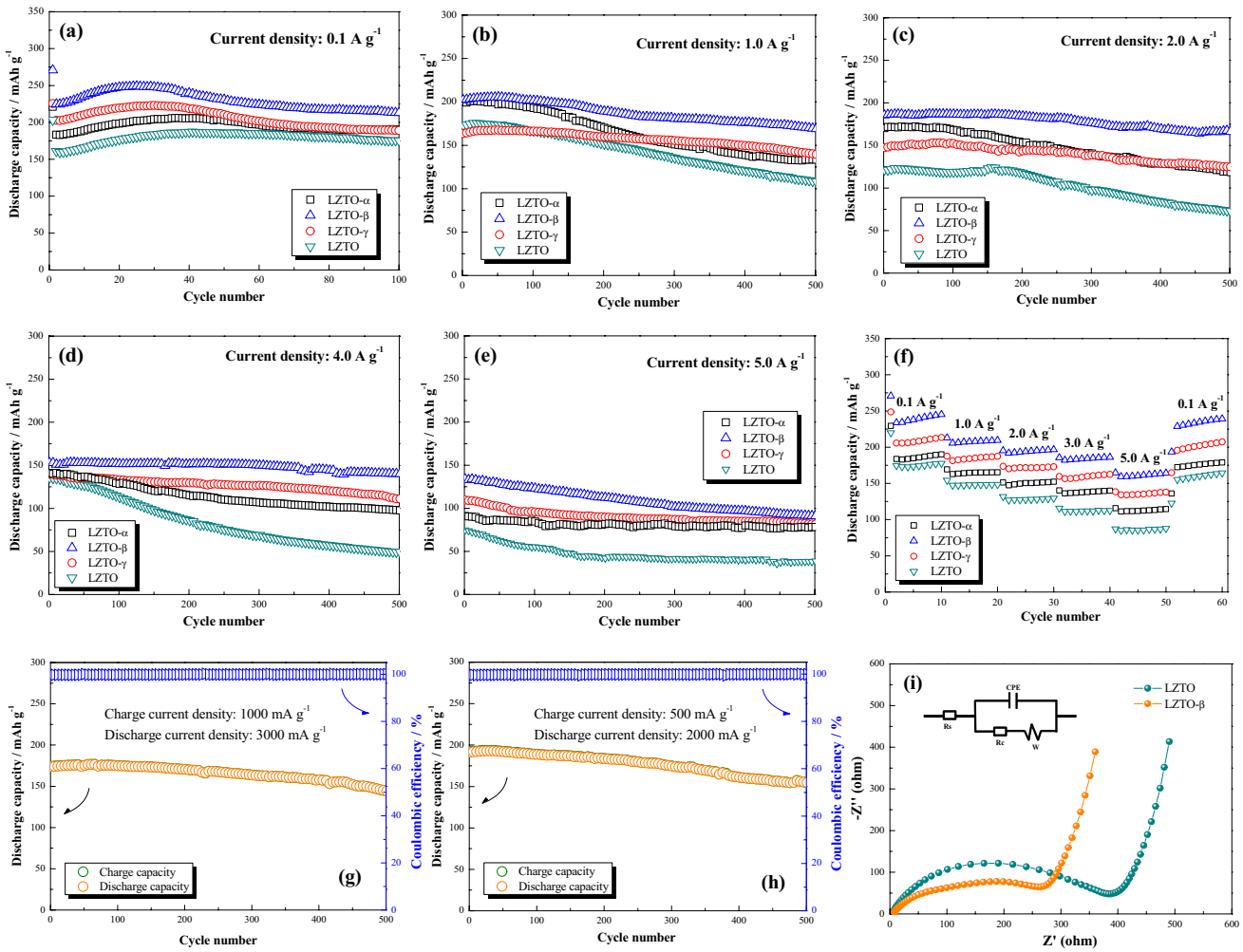

Fig. 5 Electrochemical performances of the obtained LZTO, LZTO-α, LZTO-β, and LZTO-γ samples. **a–e** Cycling performances tested at different current densities of 0.1 A g^{-1}, 1.0 A g^{-1}, 2.0 A g^{-1}, 4.0 A g^{-1}, and 5.0 A g^{-1}, respectively. **f** Rate performances tested at various current densities ranging from 0.1, 1.0, 2.0, 3.0, and 5.0, back to 0.1 A g^{-1}. **g**, **h** Cycling performances of LZTO electrode with β-cyclodextrin binder tested at different rates: charged at 1000 mA g^{-1} and discharged at 3000 mA g^{-1} and charged at 500 mA g^{-1} and discharged at 2000 mA g^{-1}. **f** Electrochemical impedance spectroscopy profiles of LZTO electrode with β-cyclodextrin and PVDF binders

binders, respectively. Moreover, the LZTO electrode with β-cyclodextrin binder does not show significant fluctuations during multiple discharge and charge cycles and has good cycling stability.

To identify the robustness of α-cyclodextrin, β-cyclodextrin, γ-cyclodextrin, and PVDF binders, rate performance of LZTO with various binders was measured at different current densities ranging from 0.1 to 5.0 A g^{-1}. As displayed in Fig. 5f, the LZTO with β-cyclodextrin binder among four samples possessed superior rate capability. Highly reversible discharge capacities of 270.8, 212.9, 195.4, 185.5, and 164.6 mAh g^{-1} were obtained at 0.1, 1.0, 2.0, 3.0, and 5.0 A g^{-1}, respectively, much higher than that of LZTO electrode with α-cyclodextrin, γ-cyclodextrin, and PVDF binders. Furthermore, the specific discharge capacity of LZTO-β electrode can quickly increase to 193.4 mAh g^{-1} when current density was returned to 0.1 A g^{-1}, which manifests good lithium intercalation and deintercalation reversibility. Therefore, the LZTO electrode with β-cyclodextrin binder displayed ultrafast lithium storage and outstanding long-term cycling stability at high current density, which showed great potential for ultrafast lithium-ion battery.

Such tremendous electrochemical performance improvement can be reasonably ascribed to the following functional group and interrelationship between compounds advantages: (1) the presence of hydroxyl groups on the surface of the external cavity in cyclodextrin, which can form hydrogen bonds with other functional groups, are beneficial to the good adhesion of LZTO electrode material with Cu current collector, improving cycling stability at high discharge–charge current densities [19, 47]; (2) the one-dimensional structure of cyclodextrin can effectively form a unique network structure between active particles; and (3) appropriate diameter of the cyclodextrin cavity is conducive to the formation of non-contact spaces between active particles, which promotes the infiltration of organic electrolyte molecule and provide the rapid lithium-ion transmission and diffusion channels.

In order to enable energy storage devices to be safely used under various conditions, it is necessary to withstand fast charge or fast discharge as an electrode active material. The results of the discharge capacities and the Coulombic efficiencies for the LZTO electrode with β-cyclodextrin binder within the voltage range of 0.05–3.0 V (versus Li/Li^+) after first cycle are shown in Fig. 5g, h. The second and the 500th discharge and charge capacities of β-cyclodextrin-based LZTO electrode are 174.2 mAh g^{-1} and 173.8 mAh g^{-1}, and 144.6 mAh g^{-1} and 144.5 mAh g^{-1}, with 99.8% and 99.9% Coulombic efficiencies, respectively, at 1000 mA g^{-1} charge and 3000 mA g^{-1} discharge (Fig. 5g). Besides, at 500 mA g^{-1} charge and 2000 mA g^{-1} discharge, the LZTO electrode with β-cyclodextrin binder exhibits an reversible capacity of 192.3 mAh g^{-1} and still gives a high reversible capacity of 154.9 mAh g^{-1} after 500 discharge–charge cycles (Fig. 5h). Furthermore, β-cyclodextrin-based electrode display better cycling stability and the capacity fading is only 0.06 mAh g^{-1} and 0.07 mAh g^{-1} per cycle within 500 cycles at discharge current densities of 3000 mA g^{-1} and 2000 mA g^{-1}. All results are shown that β-cyclodextrin-based LZTO electrode has good electrochemical performance.

To further comprehend the enhanced rates and cycling performance of the β-cyclodextrin-based LZTO electrode, we investigated the impedance of the LZTO half cells with β-cyclodextrin binder and PVDF binder via electrochemical impedance spectra measurement (EIS) measurements before cycling (Fig. 5i). The Nyquist plots of both electrodes consist of three components, electrolyte resistance (R_s), charge-transfer resistance (R_{ct}) in the high frequency region, and Warburg diffusional impedance (Z_w) at low frequency. The R_s and R_{ct} of the half-cell with β-cyclodextrin binder (7.6 Ω and 261.9 Ω) are lower than that of the half-cell with PVDF binder (7.8 Ω and 382.6 Ω). After 200 discharge–charge cycles at 1.0 A g^{-1}, the R_s and R_{ct} of the two binders increase correspondingly, but the β-cyclodextrin is still less than PVDF binder (Fig. S2). Those electrochemical impedance spectroscopy (EIS) results are again suggestive that β-cyclodextrin binder can adhere LZTO particles onto the current collector and increase transmission channels of electrons, thus reducing polarization [48].

The comparison of the present work with other reported LZTO electrodes with PVDF binder for lithium-ion batteries with long cycling test at various current densities is summarized in Table S1, demonstrating the advantages of such a water-soluble binder among the reported results.

Considering the possible changes in the molecular structure of water-soluble binder, FT-IR analysis was conducted on the β-cyclodextrin electrodes before and after cycle tests to identify the change of main functional groups. As shown in Fig. S2, the pristine β-cyclodextrin spectrum shows the characteristic absorption bands at 3378 cm^{-1} (the stretching vibration peak of -OH on the glucose ring), 2925 cm^{-1} (> CH- and $-CH_2-$ stretching vibration), 1639 cm^{-1} (> C = O stretching vibration), and 1150 cm^{-1} (-OH in-plane bending vibration). Besides, the absorption bands in the range of 1450 ~ 1350 cm^{-1} and 756 ~ 530 cm^{-1} are related to the C-O–H (C–C-H) in-plane and out-of-plane bending vibration and vibration of intramolecular ring and skeleton. These characteristic bands of pristine β-cyclodextrin exhibit few changes after the long cycle test in Fig. S3, indicating that β-cyclodextrin is stable during the charge–discharge process [19].

For the binder itself, its important function is to firmly bond the active material with the current collector so that it will not easily fall off during multiple charge–discharge cycles. To verify its firmness, we conducted multiple

bending tests. It can be seen from Figure S4 that the LZTO active material with β-cyclodextrin or PVDF as the binder is intact after 6, 15, and 30 times of bending, and it does not fall off from the current collector. This result shows that β-cyclodextrin has good fastness as a binder and is beneficial to improve electrochemical performance. To further obtain the adhesive strength of binders, the adhesion strength of LZTO with β-cyclodextrin binder and PVDF binder electrodes was investigated by peeling measurement. The detailed test process and force versus displacement graph are shown in Fig. S5. The average force required for the peeling of the LZTO with β-cyclodextrin binder (0.89 N) was higher when compared to that of LZTO with PVDF binder (0.61 N). This result further shows that β-cyclodextrin binder has better mechanical stability derived from functional groups, which is beneficial to improve cycle stability [11].

X-ray photoelectron spectroscopy (XPS) technique was further conducted to verify if there are crystal structure changes for LZTO with β-cyclodextrin or PVDF electrodes after the long cycle test. The C 1 s spectrum of LZTO with PVDF electrode in Fig. 6a presents three obvious peaks at 284.27 eV, 286.14 eV, and 290.51 eV, corresponding to $-CF_2-$, $-CH_2-$, and hydrocarbon pollutants [49, 50]. Figure 6b illustrates that the F 1 s spectrum of LZTO with PVDF electrode consists of a main peak at 687.75 eV, which corresponds to C-F bonds existing in the PVDF polymer molecular structure. In addition, after multiple intercalation and deintercalation of Li^+, the peak intensity of C-F bonds is reduced, and a new peak appeared approximately ~ 285.0 eV, which can be attributed to the corrosion of PVDF by HF [19]. The XPS results indicated that the chemical structure of PVDF binder instability during high rates charge–discharge process. Figure 6c and d present C 1 s and O 1 s

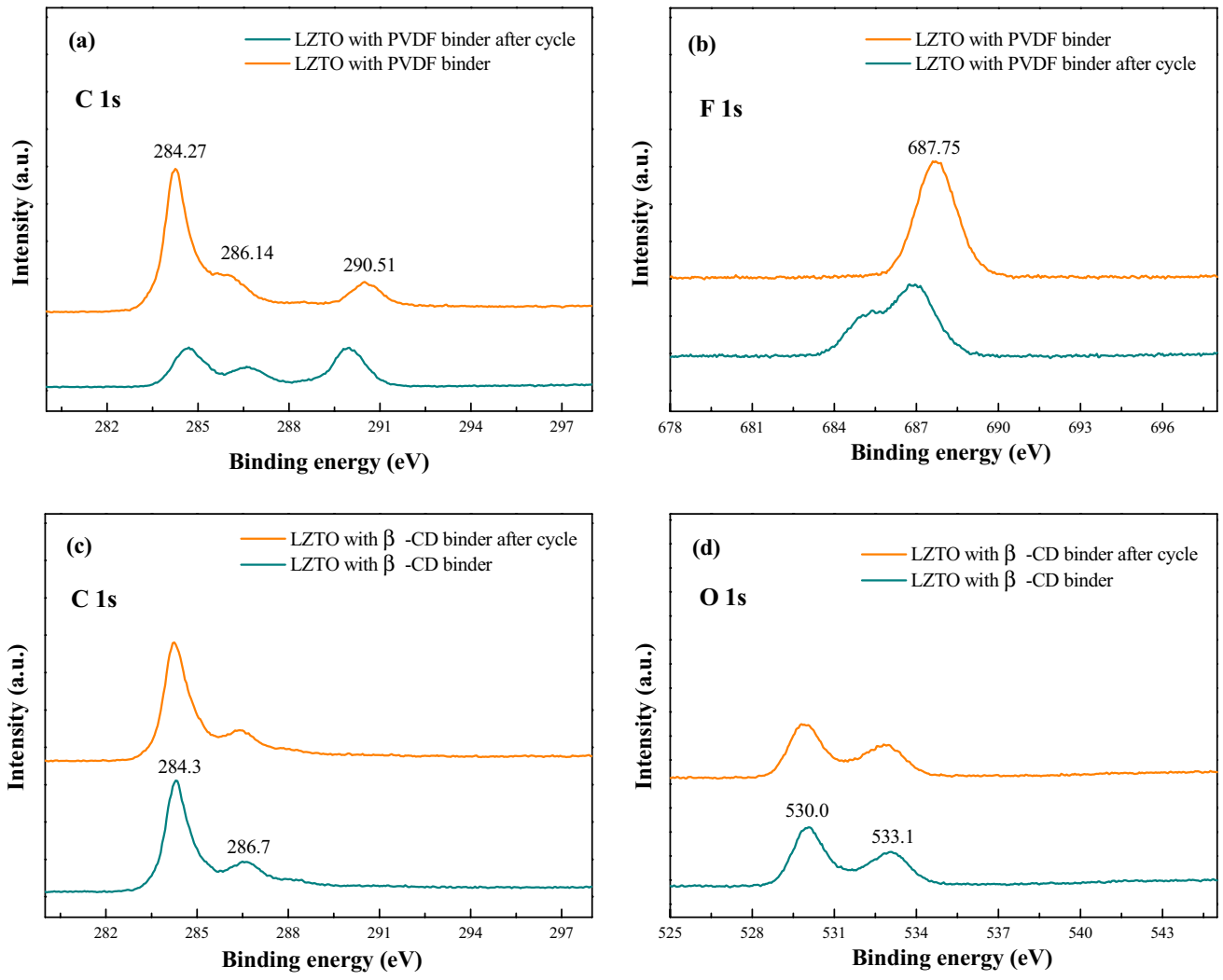

Fig. 6 XPS surface characterization of pristine electrodes and after multiple charge and discharge cycles. **a** C 1 s and **b** F 1 s spectra of LZTO with PVDF electrode. **c** C 1 s and **d** O 1 s spectra of LZTO with β-cyclodextrin electrode

spectra of LZTO with β-cyclodextrin electrode, respectively. Figure 6c illustrates the core level XPS spectrum of C 1 s, which can be fitted by two categories of binding energies: 284.3 eV corresponds to the nonoxygenated ring carbon (C–C), and 286.7 eV is associated with the oxygen-containing carbon (C–OH and O-C-O), respectively [51]. In the O 1 s XPS, the intense peak located at 530.0 eV and 533.1 eV are attributed to O-C = O and carbon oxygen single bonds (C–OH and O-C-O), respectively [40]. Compared with uncycled electrode, the peak intensity and functional group position of LZTO with β-cyclodextrin or PVDF electrode did not change significantly, and no other new impurity peaks appears after cycles, indicating that the chemical structure of β-cyclodextrin is stable during long cycle process.

In order to compare the polarization phenomenon of different electrodes intuitively, the electrode of LZTO with β-cyclodextrin and PVDF binders were evaluated by monitoring the open-circuit voltage rise of a fully discharged cell after 24 h of storage at room temperature (Fig. 7a, b). Compared with the discharge cut-off voltage, the open-circuit voltage of LZTO with β-cyclodextrin electrode is increased by 0.51 V, which is lower than that of LZTO with PVDF electrode (0.53 V), which confirms that the LZTO with β-cyclodextrin electrode has low resistance [51]. Figure 7c, d illustrates the long cycling performance of the LZTO batteries prepared with β-cyclodextrin and PVDF binders at 65 °C. The battery with the β-cyclodextrin binder exhibits good cycling stability at current densities of 1000 mA g^{-1} and 2000 mA g^{-1}, which is superior to the other one. The Coulombic efficiency of LZTO with β-cyclodextrin binder is above 97%, indicating high thermal stability. Moreover, higher discharge capacities 232.2 mAh g^{-1} (after 500 cycles) and 210.3 mAh g^{-1} (after 300 cycles) are achieved for the LZTO battery with β-cyclodextrin binder compared with that the PVDF binder (101.5 mAh g^{-1} and 82.3 mAh g^{-1}).

The batteries of LZTO with β-cyclodextrin binder and LZTO with PVDF binder were disassembled after 100 discharge–charge cycles, and the materials on the Cu current collectors were peeled off. The morphological change of LZTO with β-cyclodextrin and PVDF binders' electrodes is shown in Fig. 8. Figure 8a, b shows the SEM image of LZTO electrode with β-cyclodextrin binder, which indicates the clean surface and surface integrity of the sample. However, some by-product mixtures were covered on the

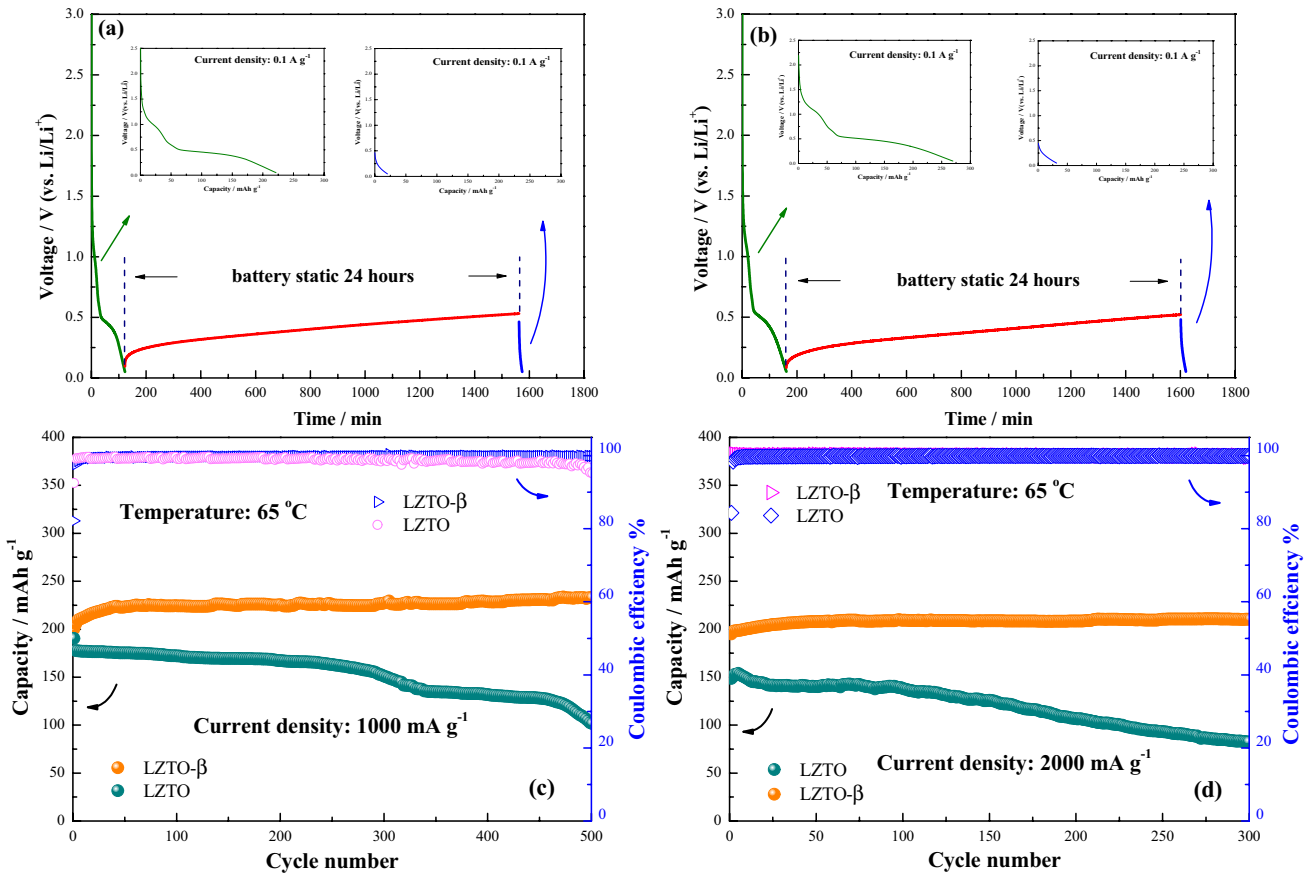

Fig. 7 **a**–**b** The storage performance evaluated by resting for 24 h after full discharge of LZTO with β-cyclodextrin and PVDF binders at room temperature. Long cycling performance of LZTO with β-cyclodextrin and PVDF binders at 65 °C; **c** 1000 mAh g^{-1} and **d** 2000 mAh g^{-1}

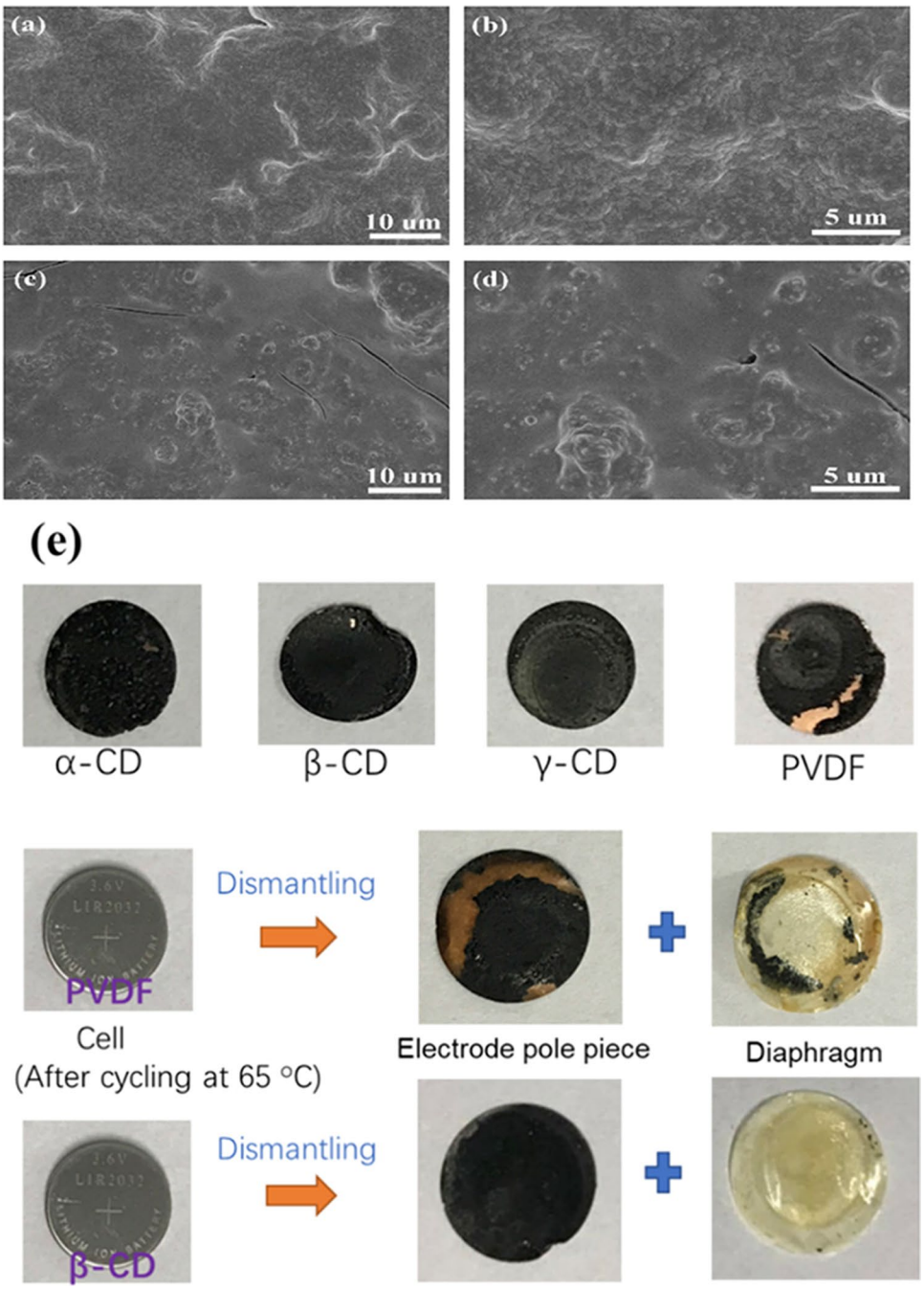

Fig. 8 SEM images of LZTO with β-cyclodextrin (**a**, **b**) and PVDF (**c**, **d**) binders after 100 discharge/charge cycles at 65 °C. **e** Images of LZTO with α-cyclodextrin, β-cyclodextrin, γ-cyclodextrin, and PVDF electrodes were taken after the delithiation at 25 °C and 65 °C

surface of the LZTO electrode with PVDF binder, and narrow fissures appear simultaneously, as shown in Fig. 8c, d. Furthermore, the electrodes were extracted from the coin cell after cycles inside the glove box to see the difference in the cycle stability at room and high temperature, and the photos of electrodes are shown in Fig. 8e. The electrode surface of LZTO with α-cyclodextrin, β-cyclodextrin, and γ-cyclodextrin binders exhibits good integrity and no significant deformation and damage after cycling at 25 °C. In contrast, the electrode surface of LZTO with PVDF binder is severely deformed including active material peeled off from the copper collector after cycling. This result indicates that the adhesion of the PVDF binder to the Cu current collector is poor. In addition, the surface of the LZTO with β-cyclodextrin binder electrode also exhibits completeness and no obvious deformation, while PVDF binder has more serious separation of active material from current collector when the ambient temperature rises to 65 °C [35, 52]. The consequence of this is that the transmission of electrons is hindered, which has an effect on the electrochemical performance. All the phenomenon indicates that the β-cyclodextrin has a stronger adhesion than the conventional PVDF binder,

and the active material is closely connected to the current collector.

Conclusion

In conclusion, the Li^+ storage capabilities of LZTO anode in lithium-ion batteries with α-cyclodextrin, β-cyclodextrin, and γ-cyclodextrin water-based binders have been systematically studied. The water-soluble binder cyclodextrin molecule contains alcoholic hydroxyl groups, which enables it to bond the active material and the current collector together, thereby improving electrochemical performance. The LZTO with β-cyclodextrin binder demonstrated the best Li^+ intercalation/deintercalation properties among all binders benefited from its unique structural characteristic and stability in electrolyte. The battery of LZTO with β-cyclodextrin binder displays higher specific capacity and good reversibility at different charge and discharge current densities. Besides, the battery with the β-cyclodextrin binder exhibits good thermal cycling stability at 65 °C, and higher discharge capacities 199.1 mAh g^{-1} (after 500 cycles) and 165.0 mAh g^{-1} (after 300 cycles) at 1000 mA g^{-1} and 2000 mA g^{-1} are achieved. Therefore, the use of β-cyclodextrin binder as a water-based binder may lead to significant improvements to the development anodes of rechargeable lithium-ion batteries.

Supplementary Information The online version contains supplementary material available at https://doi.org/10.1007/s11581-021-04374-6.

Funding This work was supported by the National Natural Science Foundation of China (Grant No. 51702081).

Declarations

Conflict of interest The authors declare no competing interests.

References

1. Armand M, Tarascon JM (2008) Building better batteries. Nature 451:652–657
2. Dunn B, Kamath H, Tarascon JM (2011) Electrical energy storage for the grid: a battery of choices. Science 334:928–935
3. Wook Choi J, Aurbach D (2016) Promise and reality of post-lithium-ion batteries with high energy densities. Nat Rev Mater 1:1–16
4. Liu Q, Su X, Lei D, Qin Y, Wen JG, Guo FM, Wu YA, Rong YC, Kou RH, Xiao XH, Aguesse F, Bareño J, Ren Y, Lu WQ, Li YX (2018) Approaching the capacity limit of lithium cobalt oxide in lithium ion batteries via lanthanum and aluminium doping. Nat Energy 3:936–943
5. Wang C, Li ZH, Liu HM, Wang YG (2017) Improved electrochemical performance of a $Li_3V_2(PO_4)_3$ cathode in a wide potential window for lithium-ion storage by surface N-doped carbon coating and bulk K-doping. New J Chem 41:8772–8780
6. Wang JJ, Sun XL (2012) Understanding and recent development of carbon coating on $LiFePO_4$ cathode materials for lithium-ion batteries. Energy Environ Sci 5:5163–5185
7. Liang GM, Peterson VK, See KW, Guo ZP, Pang WK (2020) Developing high-voltage spinel $LiNi_{0.5}Mn_{1.5}O_4$ cathodes for high-energy-density lithium-ion batteries: current achievements and future prospects. J Mater Chem A 8:15373–15398
8. Zhao BT, Deng X, Ran R, Liu ML, Shao ZP (2016) Facile synthesis of a 3D nanoarchitectured $Li_4Ti_5O_{12}$ electrode for ultrafast energy storage. Adv Energy Mater 6:1500924
9. Zhang H, Yang Y, Ren DS, Wang L, He XM (2021) Graphite as anode materials: fundamental mechanism, recent progress and advances. Energy Stor Mater 36:147–170
10. Zhong HX, He AQ, Lu JD, Sun MH, He JR, Zhang LZ (2016) Carboxymethyl chitosan/conducting polymer as water-soluble composite binder for $LiFePO_4$ cathode in lithium ion batteries. J Power Sources 336:107–114
11. Jeong YK, Kwon TW, Lee I, Kim TS, Coskun A, Choi JW (2014) Hyperbranched β-cyclodextrin polymer as an effective multidimensional binder for silicon anodes in lithium rechargeable batteries. Nano Lett 14:864–870
12. Ryou MH, Kim J, Lee I, Kim SJ, Jeong YK, Hong S, Ryu JH, Kim TS, Park JK, Lee H, Choi JW (2013) Mussel-inspired adhesive binders for high-performance silicon nanoparticle anodes in lithium-ion batteries. Adv Mater 25:1571–1576
13. Han ZJ, Yabuuchi N, Shimomura K, Murase M, Yuib H, Komaba S (2012) High-capacity Si-graphite composite electrodes with a self-formed porous structure by a partially neutralized polyacrylate for Li-ion batteries. Energy Environ Sci 5:9014–9020
14. Markevich E, Salitra G, Aurbach D (2005) Influence of the PVdF binder on the stability of $LiCoO_2$ electrodes. Electrochem Commun 7:1298–1304
15. Hwang SS, Sohn M, Park H.-Il, Choi J-M, Cho CG, Kim H (2016) Effect of the heat treatment on the dimensional stability of Si electrodes with PVDF binder. Electrochim Acta 211(356):363
16. Courtel FM, Niketic S, Duguay D, A.-Lebdeh Y, Davidson IJ (2011) Water-soluble binders for MCMB carbon anodes for lithium-ion batteries. J. Power Sources 196(2128):2134
17. Zhang Z, Zeng T, Qu C, Liu H, Jia M, Lai Y, Li J (2012) Cycle performance improvement of $LiFePO_4$ cathode with polyacrylic acid as binder. Electrochim Acta 80:440–444
18. Lux SF, Schappacher F, Balducci A, Passerini S, Winter M (2010) low cost, environmentally benign binders for lithium-ion batteries. J Electrochem Soc 157(3):A320–A325
19. Wang N, NuLi YN, Su SJ, Yang J, Wang JL (2017) Effects of binders on the electrochemical performance of rechargeable magnesium batteries. J Power Sources 341:219–229
20. Zou F, Manthiram A (2020) A review of the design of advanced binders for high performance batteries. Adv Energy Mater 10:2002508
21. Sano A, Kurihara M, Ogawa K, Iijima T, Maruyama S (2009) Decreasing the initial irreversible capacity loss of graphite negative electrode by alkali-addition. J Power Sources 192:703–707
22. Chou SL, Wang JZ, Zhong C, Rahman MM, Liu HK, Dou SX (2009) A facile route to carbon-coated SnO_2 nanoparticles combined with a new binder for enhanced cyclability of Li-ion rechargeable batteries. Electrochim Acta 54:7519–7524
23. Kim GT, Jeong SS, Joost M, Rocca E, Winter M, Passerini S, Balducci A (2011) Use of natural binders and ionic liquid electrolytes for greener and safer lithium-ion batteries. J Power Sources 196:2187–2194
24. Li J, Kloepsch R, Nowak S, Kunze M, Winter M, Passerini S (2011) Investigations on cellulose-based high voltage composite cathodes for lithium ion batteries. J Power Sources 196(18):7687–7691

25. He M, Yuan LX, Zhang WX, Hu XL, Huang YH (2011) Enhanced cyclability for sulfur cathode achieved by a water-soluble binder. J Phys Chem C 115:15703–15709
26. Zhang ZA, Bao WZ, Lu H, Jia M, Xie KY, Lai YQ, Li J (2012) Water-soluble polyacrylic acid as a binder for sulfur cathode in lithium-sulfur battery. ECS Electrochem Lett 1:A34
27. Bao WZ, Zhang ZA, Gan YQ, Wang XW, Lia J (2013) Enhanced cyclability of sulfur cathodes in lithium-sulfur batteries with Na-alginate as a binder. J Energy Chem 22:790–794
28. Pan J, Xu GY, Ding B, Han JP, Dou H, Zhang XG (2015) Enhanced electrochemical performance of sulfur cathodes with a water-soluble binder. RSC Adv 5:13709–13714
29. Qiu L, Shao ZQ, Wang DX, Wang WJ, Wang FJ, Wang JQ (2014) Enhanced electrochemical properties of $LiFePO_4$ (LFP) cathode using the carboxymethyl cellulose lithium (CMC-Li) as novel binder in lithium-ion battery. Carbohyd Polym 111:588–591
30. Gaberscek M, Bele M, Drofenik J, Dominko R, Pejovnik S (2001) Improved carbon anode properties: pretreatment of particles in polyelectrolyte solution. J Power Sources 97:67–69
31. Qiu LW, Shen YD, Fan HB, Yang XW, Wang C (2018) Carboxymethyl fenugreek gum: rheological characterization and as a novel binder for silicon anode of lithium-ion batteries. Int J Biol Macromol 115:672–679
32. Zhang ZA, Bao WZ, Lu H, Jia M, Xie KY, Lai YQ, Li J (2012) Water-soluble polyacrylic acid as a binder for sulfur cathode in lithium-sulfur battery. ECS Electrochem Lett 1(2):A34–A37
33. Komaba S, Yabuuchi N, Ozeki T, Okushi K, Yui H, Konno K, Katayama Y, Miura T (2010) Functional binders for reversible lithium intercalation into graphite in propylene carbonate and ionic liquid media. J Power Sources 195:6069–6074
34. Park HK, Kong BS, Oh ES (2011) Effect of high adhesive polyvinyl alcohol binder on the anodes of lithium ion batteries. Electrochem Commun 13:1051–1053
35. Tang HQ, Weng Q, Tang ZY (2015) Chitosan oligosaccharides: a novel and efficient water soluble binder for lithium zinc titanate anode in lithium-ion batteries. Electrochim Acta 151:27–34
36. Kovalenko I, Zdyrko B, Magasinski A, Hertzberg B, Milicev Z, Burtovyy R, Luzinov I, Yushin G (2011) A major constituent of brown algae for use in high-capacity Li-ion batteries. Science 333:75–79
37. Ohta N, Sogabe T, Kuroda K (2001) A novel binder for the graphite anode of recharge-able lithium ion batteries for the improvement of reversible capacity. Carbon 39(9):1434–1436
38. Liu J, Zhang Q, Sun Y-K (2018) Recent progress of advanced binders for Li-S batteries. J Power Sources 396:19–32
39. Liu J, Sun MH, Zhang Q, Dong FF, Kaghazchi P, Fang YX, Zhang SQ, Lin Z (2018) A robust network binder with dual functions of Cu^{2+} ions as ionic crosslinking and chemical binding agents for highly stable Li-S batteries. J Mater Chem A 6:7382–7388
40. Hu LL, Zhang XD, Li B, Jin MH, Shen XH, Luo ZW, Tian ZY, Yuan LZ, Deng JK, Dai ZF, Song JX (2021) Design of high-energy-dissipation, deformable binder for high-areal-capacity silicon anode in lithium-ion batteries. Chem Eng J 420:129991
41. Jiao XX, Yin JQ, Xu XY, Wang JL, Liu YY, Xiong SZ, Zhang QL, Song JX (2020) Highly energy-dissipative, fast self-healing binder for stable Si anode in lithium-ion batteries, Adv Funct Mater. 2005699
42. Hu LL, Zhang XD, Zhao PY, Fan H, Zhang Z, Deng JK, Ungar G, Song JX (2021) Gradient H-bonding binder enables stable high-areal-capacity Si-based anodes in pouch cells. Adv Mater. 2104416
43. Liu T, Tang HQ, Liu JY, Pu YJ, Zhang J, Lu ZW, Li W, Tang ZY, Ding F (2018) Improved electrochemical performance of $Li_2ZnTi_3O_8$ using carbon materials as loose and porous agent. Electrochim. Acta 259:28–35
44. Miao XW, Ni H, Zhang H, Wang CG, Fang JH, Yang G (2014) Li_2ZrO_3-coated 0.4 $Li_2MnO_3{\cdot}0.6LiNi_{1/3}Co_{1/3}Mn_{1/3}O_2$ for high performance cathode material in lithium-ion battery. J. Power Sources 264:147–154
45. Ge H, Li N, Li D, Dai C, Wang D (2008) Electrochemical characteristics of spinel $Li_4Ti_5O_{12}$ discharged to 0.01 V. Electrochem. Commun. 10:719–722
46. Borghols WJH, Wagemaker M, Lafont U, Kelde EM, Mulder FM (2009) Size effects in the $Li_{4+x}Ti_5O_{12}$ spinel. J. Am Chem. Soc. 131:17786–17792
47. Nguyen MHT, Oh E-S (2015) Improvement of the characteristics of poly(acrylonitrile–butylacrylate) water-dispersed binder for lithium-ion batteries by the addition of acrylic acid and polystyrene seed. J Electroanal Chem 739:111–114
48. Qin JL, Zhu HL, Lun N, Qi YX, Bai YJ (2020) $Li_2ZnTi_3O_8$/C anode with high initial Coulombic efficiency, long cyclic life and outstanding rate properties enabled by fulvic acid. Carbon 163:297–307
49. Kuvshinov A, Pesin L, Chebotaryov S, Kuznetsov M, Evsyukov S, Sapozhnikova T, Mirzoev A (2008) Kinetics of radiation-induced carbonization of poly(vinylidene fluoride) film surface. Polym Degrad Stab 93:1952–1955
50. El Mohajir B-E, Heymans N (2001) Changes in structural and mechanical behaviour of PVDF with processing and thermomechanical treatments. 1 Change in structure. Polymer 42:5661–5667
51. Wang F, Borodin O, Gao T, Fan XL, Sun W, Han FD, Faraone A, Dura JA, Xu K, Wang CS (2018) Highly reversible zinc metal anode for aqueous batteries. Nat Mater 17:543–549
52. Ai LH, Gao XY, Jiang J (2014) In situ synthesis of cobalt stabilized on macroscopic biopolymer hydrogel as economical and recyclable catalyst for hydrogen generation from sodium borohydride hydrolysis. J Power Sources 257:213–220